



UNIVERSITÀ POLITECNICA DELLE MARCHE
Repository ISTITUZIONALE

MIMO 4 X 4 vs. MIMO 2 X 2 performance assessment of a real life LTE base station in a reverberation chamber

This is the peer reviewed version of the following article:

Original

MIMO 4 X 4 vs. MIMO 2 X 2 performance assessment of a real life LTE base station in a reverberation chamber / Micheli, D.; Barazzetta, M.; Bastianelli, L.; Diamanti, R.; Carlini, C.; Colombo, M.; Moglie, F.; Mariani Primiani, V.. - In: AEÜ. INTERNATIONAL JOURNAL OF ELECTRONICS AND COMMUNICATIONS. - ISSN 1434-8411. - ELETTRONICO. - 129:(2021). [10.1016/j.aeue.2020.153500]

Availability:

This version is available at: 11566/289300 since: 2024-04-24T18:37:25Z

Publisher:

Published

DOI:10.1016/j.aeue.2020.153500

Terms of use:

The terms and conditions for the reuse of this version of the manuscript are specified in the publishing policy. The use of copyrighted works requires the consent of the rights' holder (author or publisher). Works made available under a Creative Commons license or a Publisher's custom-made license can be used according to the terms and conditions contained therein. See editor's website for further information and terms and conditions.

This item was downloaded from IRIS Università Politecnica delle Marche (<https://iris.univpm.it>). When citing, please refer to the published version.

note finali coverage

(Article begins on next page)

POST PRINT VERSION

Title: MIMO 4x4 vs. MIMO 2x2 Performance Assessment of a Real Life LTE Base Station in a Reverberation Chamber

Authors: Davide Micheli, Massimo Barazzetta, Luca Bastianelli, Riccardo Diamanti, Camillo Carlini, Michele Colombo, Franco Moglie, Valter Mariani Primiani

DOI: 10.1016/j.aeue.2020.153500

Reference: S1434-8411(20)31197-3

Editor Website: <https://www.sciencedirect.com/science/article/pii/S1434841120311973>

Received Date: 2 June 2020

Accepted Date: 13 October 2020

Available online: 7 November 2020

Please cite this article as: D. Micheli, M. Barazzetta, L. Bastianelli, R. Diamanti, C. Carlini, M. Colombo, F. Moglie, V. Mariani Primiani, MIMO 4x4 vs. MIMO 2x2 Performance Assessment of a Real Life LTE Base Station in a Reverberation Chamber, International Journal of Electronics and Communications (2021), doi: <https://doi.org/10.1016/j.aeue.2020.153500>

Copyright © 2020 Published by Elsevier GmbH.

MIMO 4x4 vs. MIMO 2x2 Performance Assessment of a Real Life LTE Base Station in a Reverberation Chamber

Davide Micheli^a, Massimo Barazzetta^b, Luca Bastianelli^{c,*}, Riccardo Diamanti^d, Camillo Carlini^a, Michele Colombo^b, Franco Moglie^c and Valter Mariani Primiani^c

^aTIM S.p.A., Via Oriolo Romano, 240, Building B, 00189 Rome, Italy

^bNokia Networks Italia, Energy Park 14, 20871 Vimercate, Italy

^cDipartimento di Ingegneria dell'Informazione, Università Politecnica delle Marche, via Breccie Bianche 12, 60131 Ancona, Italy

^dTIM S.p.A., Via Guido Miglioli 11, 60131 Ancona, Italy

ARTICLE INFO

Keywords:

LTE, MIMO 4x4, RSRP, SINR, throughput.

ABSTRACT


The performance of a MIMO 4×4 transmission solution applied to 4th generation LTE FDD technology are evaluated inside a reverberation chamber (RC) to quantify its benefit against the LTE typical MIMO 2×2 transmission scheme, in different environment conditions. The implementation of MIMO 4×4 in live networks requires the connection of two additional cables between base station transmitters and antennas, and operators face additional costs. Throughput and modulation code scheme allocation are analyzed as a function of the signal to interference-plus-noise ratio (SINR), for both indoor and outdoor environments. Experimental results in a live network are compared to those obtained in the RC of our laboratory. Results highlight that MIMO 4×4 is convenient for SINR greater than 10–15 dB. These results can help mobile network operators to evaluate if the expected benefit justifies the additional costs in an operating actual network.

1. Introduction

Reverberation chambers (RC) are resonant enclosures that operate with a large amount of modes excited at the same time. This overmoded condition contributes to establish an electromagnetic field statistically uniform, isotropic and without a preferable polarization (1). In an RC, the stochastic nature of the fields (2) is useful in electromagnetic compatibility (EMC) testing (3).

Assuming wireless communication systems operating into a real environment, they face very complex propagation conditions, with many reflections that can become strongly uncorrelated in urban and indoor environments, due to the presence of moving scattering objects and peoples. These real propagation conditions are more similar to what happens inside an RC w.r.t an anechoic chamber adopted in classical tests. An RC is used to reproduce different propagation environments by controlling the multipath amount (4; 5) with no unwanted effects due to external interfering signals. For example, the 3GPP test specification TS37.544 (6) includes RC as one of the methodologies for total radiated power (TRP) and for total isotropic sensitivity (TIS) certification testing of handsets. Data throughput (TP) is a common metric for evaluating the performance of multiple-input-multiple-output (MIMO) devices. It can be evaluated in the RC, as outlined in the 3GPP technical report TR37.977 (7). The RC is particularly useful for evaluating the performance of MIMO devices because they are optimized for multipath environments (8; 9). The RC was adopted to assess the passive antenna performance under MIMO configuration (10), and for over-the-air test (OTA) of MIMO devices (4), also considering the possibility to control testing uncertainty (5; 11). Typically, an RC is used in conjunction with channel emulators (12) to improve the device testing. By adopting a long

*Corresponding author: l.bastianelli@pm.univpm.it

 davide.micheli@telecomitalia.it (D. Micheli); massimo.barazzetta@nokia.com (M. Barazzetta); l.bastianelli@pm.univpm.it (L. Bastianelli); riccardo.diamanti@telecomitalia.it (R. Diamanti); camillo.carlini@telecomitalia.it (C. Carlini); michele.colombo@nokia.com (M. Colombo); f.moglie@univpm.it (F. Moglie); v.mariani@univpm.it (V. Mariani Primiani)

ORCID(s):

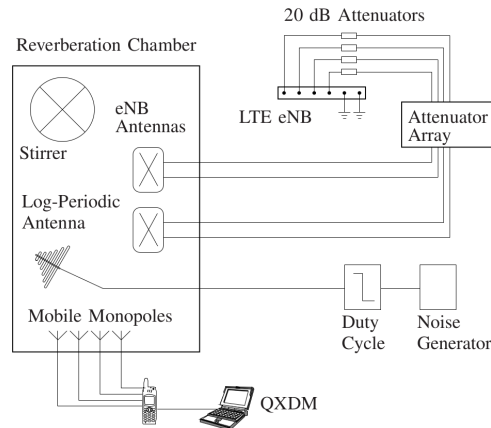


Figure 1: Schematic description of the set-up.

term evolution (LTE) base station (BS) emulator, RC testing has been extended to last generation of LTE devices (13).

Recently, complete OTA tests have been carried out on a real-life LTE BS (14). It was the first time that a real live BS was used instead of a BS emulator. It allowed also to check TP under hostile conditions in both downlink (14) and uplink (15) directions. The RC was successfully adopted to verify some important features of the real BS LTE, such as the carrier aggregation capability (16). Currently, fourth generation mobile networks are implemented today with MIMO 2×2 with transmission modes 3 or 4 (TM3 or TM4).

The upgrade to higher order MIMO transmissions – like 4×4 – requires additional hardware. Two additional transmitters and cables must be added to the existing radio infrastructure of the cell. Before the hardware upgrading to MIMO 4×4 , the knowledge of expected benefits in terms of signal strength – here referred as reference signal received power (RSRP) – and signal to interference plus noise ratio (SINR) is of fundamental importance for mobile network operators. Benefits can depend on different propagation conditions (such as outdoor, commercial indoor or residential indoor)

In this paper, we present the results of an experimental campaign executed in the RC of the Università Politecnica delle Marche, in cooperation with Telecom Italia and Nokia, focused on the evaluation of such benefits. In section II, the entire experimental set-up is described, the RC, the BS and the LTE mobile test receiver. Moreover, the RC conditions to obtain indoor and outdoor propagation are reported too. In section III main results are reported and discussed comparing MIMO 2×2 and MIMO 4×4 performances in outdoor and indoor propagation scenario. Modulation and Coding Scheme (MCS) are evaluated as function of SINR and in relation to transmitted power. In section IV the effect of multipath on MIMO allocation and performance is evaluated. To do so, throughput performance is compared between different chamber conditions. In section V some considerations about TIM live network implementation of MIMO 4×4 and MIMO 2×2 as a function of bandwidth are reported.

2. Set-up description

OTA tests are carried out inside an RC with dimensions $6.0 \times 4.0 \times 2.5 \text{ m}^3$ equipped by a z-folded stirrer having a rotation diameter of 1.5 m and a height of 2.4 m. Its rotation axis is vertical. The chamber is equipped with another stirrer with a horizontal rotation axis. During all the measurements, it was not used and acts as a diffuser only. Figure 1 summaries all connections among adopted instrumentation.

A BS NOKIA model Flexi Multiradio feeds the chamber through an array of precision attenuators (R&S HOSM 2×4) connected to two antennas. Attenuators are by a remote PC in order to dynamically change the signal levels of the radio environment. In that way, it is possible to accurately adjust the signal level for each of the four branches of the BS transmitter. Each antenna panel (Kathrein 80010677) contains two cross polarized antennas operating in the range 1710 – 2700 MHz as visible in detail in Figure 2. Beside the BS LTE signal, an interference signal is injected into the RC by a log-periodic antenna (Schwarzbeck

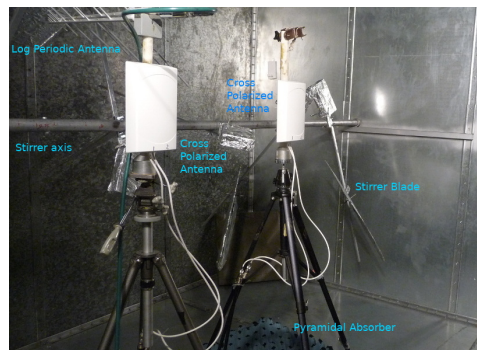


Figure 2: Picture of the antennas connected to the BS and the log-periodic antenna connected to the noise generator.

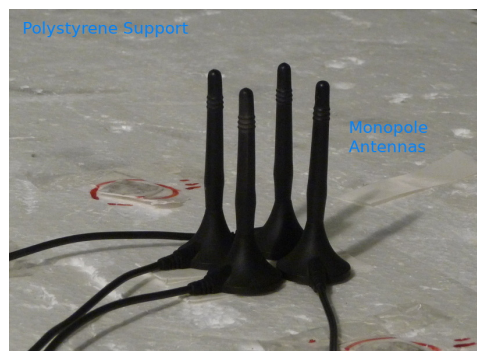


Figure 3: The four antennas of the mobile station. The picture shows the case when the monopole antennas are placed very closed each other. The length of each monopole is 9 cm.

USLP 9143-300) as visible in Figure 2. A carrier of 1835 MHz – the same frequency of the BS downlink band – is modulated by an additive white Gaussian noise (AWGN) with a 20 MHz bandwidth. The aim of the presence of this AWGN generator (R&S model SMBV 100A) is the emulation of real-life situations where the mobile station operates in a noisy environment. In order to make this interference more realistic, an ON-OFF low frequency amplitude modulation is added. This additive low frequency modulation is provided by a PIN diode modulator (HP 11665B) and a pulse generator (HP 8011A) set to a frequency of 1 kHz and with a pulse duration of 250 μ s. We chose this value since the total duration of the LTE symbol is 71.4 μ s and 14 symbols compose one TTI (1 ms). Thus, applying a pulse of 250 μ s with 1 kHz frequency, there is the 25% probability for each LTE symbol to be affected by noise (15). The selected user equipment is a Qualcomm test device – both MIMO 4 \times 4 and 256 QAM capable – model MSM8996/8998, traced with Qualcomm Extensible Diagnostic Monitor (QXDM) characterized by four input connectors for external antennas at the desired band. Since it is a specific prototype and its enclosure is not completely shielded, it is positioned outside the RC to avoid a direct coupling between the BS (and AWGN noise) into the phone circuitry. Therefore, four monopole antennas are located inside the chamber and the signal is carried out to the mobile station by four feed-through connectors, Figure 3. Different antenna reciprocal distances and both vertical and horizontal polarizations are considered. The BS is directly connected to the live network of the Telecom Italia Mobile (TIM) operator. All transmission data measurements (RSRP, modulation order, SINR, rank indication, throughput, etc.) are downloaded and analyzed on an external PC by the QXDM software. Figure 4 shows a complete view of both the inner and the outer of the RC. The well visible absorbing material is inserted in the RC to replicate typical indoor and outdoor multipath propagation conditions (17; 18). The quality factor reduction allows us to tune the power delay profile (PDP) and consequently the time delay spread and the K-factor (19; 20; 21; 22).

More precisely, we characterized the chamber in terms of S_{21} measurement between transmitting and receiving antennas. The chamber impulse response $h(t) = \text{IFT}(S_{21})$ is achieved by an inverse Fourier



Figure 4: Pictures of the inner and the outer view of the RC.

transform (IFT). The PDP is computed by averaging the impulse response for many stirrer angles.

$$\text{PDP} = \left\langle |h(t)|^2 \right\rangle_N, \quad (1)$$

where $\langle \cdot \rangle_N$ means the ensemble average over the N stirrer positions. The time delay spread τ_{RMS} is computed from the PDP.

$$\tau_{\text{RMS}} = \frac{\sqrt{\int_0^\infty (t - \tau_{\text{ave}})^2 \text{PDP}(t) dt}}{\int_0^\infty \text{PDP}(t) dt}, \quad (2)$$

where

$$\tau_{\text{ave}} = \frac{\int_0^\infty t \text{PDP}(t) dt}{\int_0^\infty \text{PDP}(t) dt}. \quad (3)$$

In applying (1) we introduced a threshold of -30 dB as suggested in (23). This parameter allows to relate RC measurements to real life environment.

The Q factor is calculated from the S_{21} (3).

$$Q = \frac{16\pi^2 V \left\langle |S_{21}|^2 \right\rangle_N}{\eta_{TX} \eta_{RX} \lambda^3}, \quad (4)$$

where V is the volume, λ the free-space wavelength, η_{TX} and η_{RX} are the transmitting and receiving antenna total efficiencies, respectively.

The availability of an accurate Q-factor value, allows to recover the chamber coherence bandwidth B_c (20; 24; 19; 25).

$$B_c = \frac{f}{Q}. \quad (5)$$

Finally, the addition of absorbing materials reduces the scattered energy compared to the direct energy between TX and RX antennas. This is quantified by the Rician K-factor which is the ratio between direct and scattered energy (21)

$$K = \frac{\left\langle |S_{21}|^2 \right\rangle}{\left\langle |S_{21} - \langle S_{21} \rangle|^2 \right\rangle}. \quad (6)$$

Table 1

RC parameters for each loading condition at 1835 MHz.

	Q-factor	τ_{RMS} (ns)	K-factor	B_c (kHz)
EC	30 385	1347	0.054	62
MC	7 283	370	0.199	257
HL	2 951	163	0.491	635
VHL	957	67	0.723	1959
UHL	771	54	0.974	2432

Table 2

Tuning of noise power spectral density (dBm/Hz) for each loading condition.

UHL	VHL	HL	MC	EC
OFF	OFF	OFF	OFF	OFF
-45	-60	-44	-68	-74
-40	-55	-39	-63	-69
-35	-50	-34	-58	-64
-30	-45	-29	-53	-59
-25	-40	-24	-48	-54
-20	-35	-19	-43	-49
-15	-30	-14	-38	-44
-10	-25	-9	-33	-39
-5	-20	-5	-28	-34

It increases when the chamber is loaded.

The RSRP is set to replicate a signal strength that is typical of outdoor environments (-80 dBm) or indoor environments (-100 dBm), see again (17; 18). Moreover, the noise and the signal strength are further adjusted to follow the quality factor variation due to absorber insertion: empty chamber (EC), medium load (ML), high load (HL) and very high load (VHL). The purpose is to maintain always the same working points for RSRP (-80 dBm outdoor, -100 dBm indoor) and possibly, the same SINR changing the loading condition. Besides the previously adopted RC conditions (14; 15), we add a ultra high load (UHL) condition by inserting 4 pyramidal absorbers Emerson&Cuming VHP-18-NRL, 10 pyramidal absorbers Emerson&Cuming VHP-8-NRL, 8 Emerson&Cuming ANW-77. As an example, Figure 5 shows the PDP in all loading conditions and Table 1 reports all chamber parameters whereas Table 2 reports the noise power spectral density set for each loading condition. Besides setting up the RC with the above loading conditions, the stirrer rotating speed is set to replicate the fading of a typical outdoor (30 deg/s) and indoor (60 deg/s) environment. The RC rotating speed was tuned by comparing the behavior of the RSRP fast Fourier transform (FFT) and to find the best match between them. One is the RC signal and the others were recorded in live network environments, as example: cafeterias, hotel lobbies, or open space. Figure 6 represents that comparison. The comparison was performed in the frequency domain. In fact, the spectrum analysis better compares the profile behavior of the periodic RSRP in the RC with that of real environments. The stirrer rotating speed was set to fit the both signals. The small deviation in the lower part of the spectrum is due to slow fluctuations of real environment RSRP that cannot be reproduced by the RC in the measurement time interval.

3. Expected benefits from MIMO 4×4

The usage of TM3 or TM4 in classic MIMO 2×2 transmission schemes brings some differences in throughput performance especially at low SINR values, thanks to the different implementation of precoding.

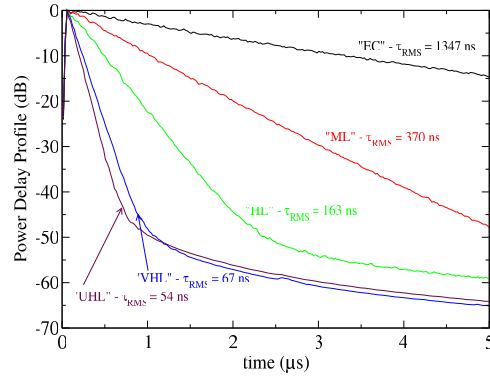


Figure 5: Power delay profile for each chamber loading condition.

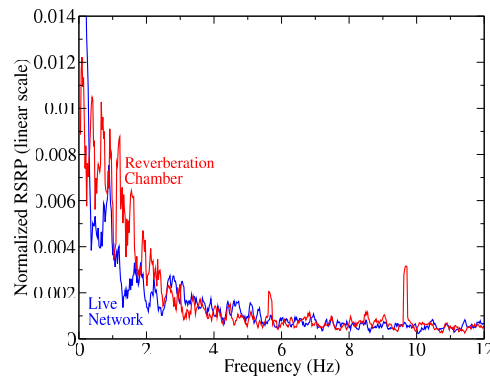


Figure 6: Indoor case: comparison in the frequency domain between a live network signal and a signal replicated in the RC. The two RSRP values are normalized to have the same energy.

When moving to MIMO 4×4 , the number of layers is doubled and the precoding is chosen among sixteen possible values, instead of the four values of the classic MIMO 2×2 solution. In this testing campaign only TM4 is considered for the MIMO 4×4 case. This means that the throughput can be theoretically doubled and precoding is more accurate and more effective for the radio channel.

The BS adapts the transmission to the radio conditions by using the channel quality indicator (CQI), the precoder matrix indication (PMI) and the rank indication (RI) reported by mobile station. These measurements are used by the BS in order to adapt to the radio channel, but they could be further compensated based on layer 1 hybrid automatic repeat requests (HARQ) feedbacks and block error rate (BLER) targets. Whenever possible, the addition of the third and fourth branches is normally done re-using the radio cables that are already present on site to serve other technologies inserting the LTE signal in the existing cables by means of diplexers. This reduce implementation costs as the existing infrastructure is re-used, but an additional implementation work is required.

Figure 7 and Figure 8 show the rank and the modulation order, respectively. They are selected based on the CQI and RI received from the user equipment (UE), typically known as “mobile device” or “smartphone”. MIMO 4×4 introduces the support of rank 3 (three transmission layers) and rank 4 (four transmission layers). Rank 4 is allocated when SINR is higher than 20 dB. Rank 3 is allocated when SINR is within 10 and 20 dB. Below 10 dB, only rank 1 and rank 2 are used and the benefit of MIMO 4×4 is negligible. However, higher layers ranks (3 and 4) persist until $\text{SINR} \geq 10$ dB, providing relevant benefits to the end-user throughput in this situation.

On the other hand, 256 QAM is allocated only when the SINR is higher than 20 dB. This is due to the higher error rate that may affect 256 QAM constellation in poor radio conditions, since the symbols are very close to each other. The overall power transmitted by the LTE cell is doubled. In some cases, the operator

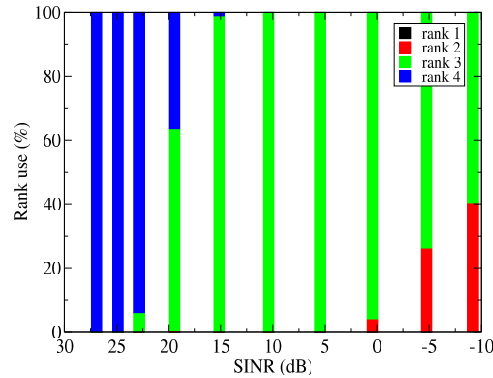


Figure 7: Rank allocated by the mobile station, MIMO 4 × 4.

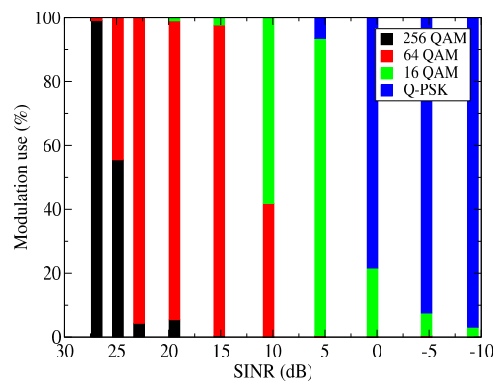


Figure 8: Modulation order allocated by the BS, MIMO 4 × 4.

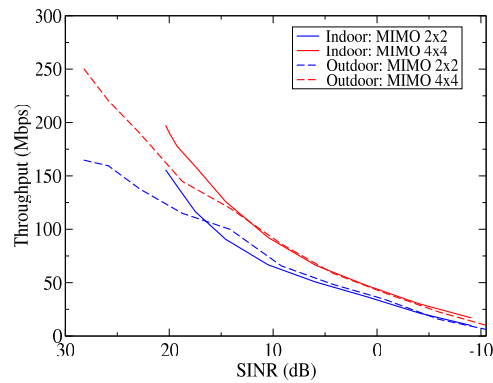


Figure 9: Outdoor (continuous line) and indoor (dashed line) cases: throughput comparison as function of SINR.

is limited on the maximum transmission power in order to fulfill national limits for generic public exposure to electromagnetic field. Moreover, the BS transmission power cannot be increased excessively. In fact, the limited UE power budget could cause the uplink connection to fail when located at cell edge.

The present paper focus on the benefits introduced by the MIMO 4 × 4 implementation vs existing MIMO 2 × 2, in different radio conditions. Figure 9 compares the throughput of these solutions in outdoor and indoor conditions, with RSRP = −80 dBm and variable SINR. In the outdoor case, the benefits in terms of throughput (measured at packet data convergence protocol (PDCP) layer) is that of +52% for the peak throughput and +35% for the average throughput. It is also clearly visible from the picture that the

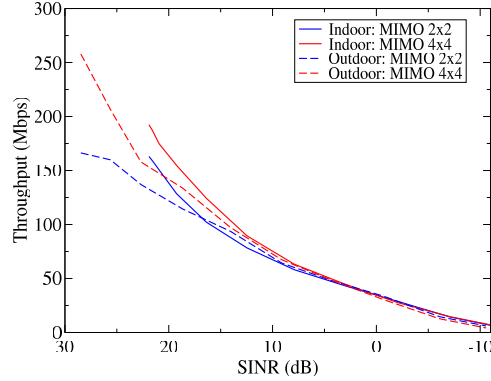


Figure 10: Outdoor (continuous line) and indoor (dashed line) cases: throughput comparison as function of SINR. The same overall transmitted power is maintained.

benefits are more remarkable when the SINR (in this picture the SINR for the MIMO 2×2 case is taken as a reference) tends to high values. Similar results could be drawn for the indoor cases, but with slightly different numbers.

Therefore, also the scenario where the MIMO 4×4 solution is enabled, maintaining the same overall transmission power (thus, halving the transmission power of each branch), has been tested and results are presented in Figure 10. In the outdoor case, the throughput improvement is smaller and could be quantified as +55% of peak throughput and +21% on average. Moreover, to have remarkable effects from MIMO 4×4 implementation, the SINR need to be greater than 14 dB. In the indoor case, the improvement from MIMO 4×4 introduction decreases, where the multipath is not rich as in the outdoor case.

This environment is reproduced with a chamber loaded to the VHL condition and fed to reach a RSRP level of -100 dBm. The peak throughput increases of about 27% while the average throughput increases of about 31%. Benefits are still visible and more remarkable when SINR tends to high values. MIMO solutions will also be relevant for the deployment of mmWave mobile networks (26; 27). When halving the transmission power of each branch to transmit with the same overall cell power of MIMO 2×2 , the throughput improvements are reduced to 18% (peak) and 16% (average) and the benefits are remarkable when the SINR is above 14 dB.

4. Effect of multipath on MIMO 4×4 allocation

Another scope of the test campaign is to evaluate the effect of multipath on MIMO allocation and performance. To do so, we compare throughput performance between different chamber conditions. When we move from one loading condition to the other, the signal strength as well as noise and interference – and consequently SINR – change as well. Signal strength could be easily adjusted to a common value (for example: -100 dBm) with the aid of the attenuator array, and the noise could be set, in a first instance, based on the quality factor, as mentioned above (Table 2). Nevertheless, SINR may change in unpredictable ways since the level of interference is not set by us, being determined by the chamber conditions. Thus, a first test is executed to measure the SINR values recorded in two different chamber conditions, setting the noise as indicated in Table 2. Then, the noise is further adjusted by the difference of the SINR in the two chamber conditions and the test is repeated. For example, if we want to compare the MIMO 4×4 performance at high load (HL) chamber conditions versus the performance at very high load (VHL) conditions, we will have to apply a following additional compensation to values in Table 2, after having measured the SINR difference in the first iteration.

$$\Delta N^{HL} = \text{SINR}_1^{HL} - \text{SINR}_1^{VHL} . \quad (7)$$

We concentrate on the VHL and HL loading conditions, as these are the ones representing a typical indoor or outdoor propagation (see (17; 18)). Signal strength is set equal to -100 dBm for both cases. The effect of the compensation is visible in Figure 11, where SINR values are plotted against noise injected in

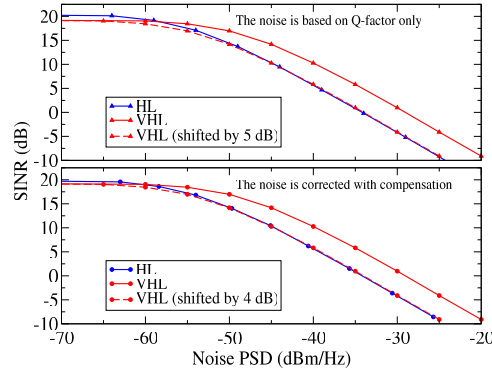


Figure 11: SINR for HL and VHL conditions. The noise is injected at first iteration and is based on Q-factor only (upper plot) or is corrected with additional compensation (lower plot).

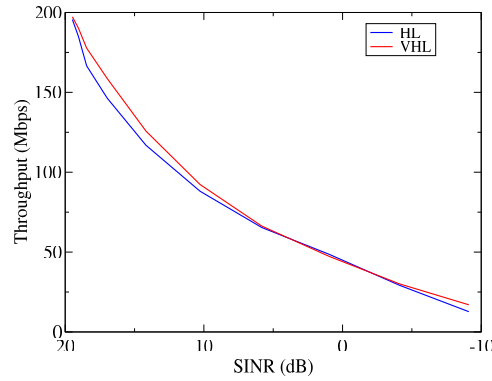


Figure 12: Throughput for the MIMO 4 × 4 configuration, HL and VHL conditions, same SINR.

chamber at first iteration and after the compensation. The compensation shows a light improvement that is visible translating the VHL curves in order to overlap them with the HL ones. Since SINR trend at HL and VHL conditions is almost the same after the compensation, we may conclude that any difference experienced on throughput is to be ascribed to multipath only. In few words, the different contribution of interference presented by the two cases is compensated with additional noise to have the same SINR for all noise samples. The throughput for the HL environment and the VHL environment (measured at same SINR after compensation) is shown in Figure 12. It is quite remarkable how the interference (multipath) may play a role in affecting the performance. MIMO 4 × 4 presents better improvements at HL conditions compared with MIMO 2 × 2 (see Figure 9) and the rich multipath condition (HL vs VL) slightly reduce the throughput as reported in Figure 12. This could be quantified as a 10% degradation in throughput when the SINR is between 12 dB and 18 dB.

5. Live network implementation of MIMO 4 × 4

In the Italian regions Emilia-Romagna and Veneto the MIMO 4 × 4 has been implemented. Key performance indicator (KPI) values of all eNB are available during all the day. We compare the data for July 2018 with those of MIMO 2 × 2 obtained for cells of similar typology. Figure 13 and Figure 14 compare the probability density functions of some MIMO 4 × 4 and MIMO 2 × 2 configurations. Throughput distribution is reported for LTE cells of different bands (band-3: 1800 MHz, 20 MHz bandwidth; band-7: 2600 MHz, 15 MHz bandwidth; band-20: 800 MHz, 10 MHz bandwidth) and different MIMO configurations (2 × 2 or 4 × 4). These are obtained from statistical counters retrieved from the network supervision system. Figure 13 shows the downlink throughput distribution, where for both band-7 cells (light green and green curves) we can notice a light shift toward higher throughput values when moving to MIMO 4 × 4. The same happens

about band-3 cells (orange and red curves). In in live network, it is noticeable that the improvements on throughput distribution is smaller than in laboratory environment. The reason is that the throughput measured by network counters is affected by radio conditions, applications running on smartphones, and user activity.

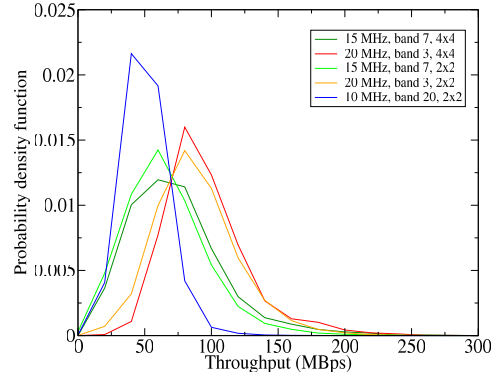


Figure 13: Probability density function in the downlink case for the throughput of some MIMO 4×4 and MIMO 2×2 configurations. Data where measured in the month of July 2018 in the TIM live network.

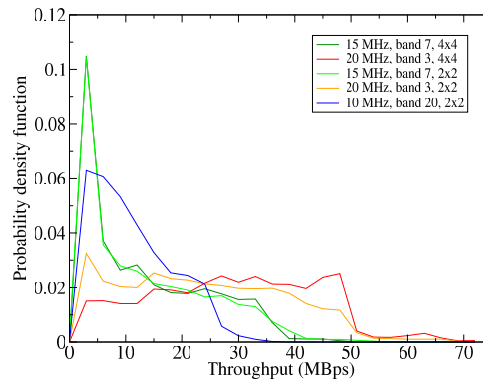


Figure 14: Probability density function in the uplink case for the throughput of some MIMO 4×4 and MIMO 2×2 configurations. Data where measured in the month of July 2018 in the TIM live network.

Moreover it depends on MIMO capability of smartphones and by their distribution with respect to the radio BS. Figure 14 shows a similar distribution, but for the uplink throughput. MIMO 2×2 or 4×4 is a concept nowadays applicable only in the LTE downlink direction, but some side effects could be visible also in the uplink, when applications used by smartphones are based on confirmed protocols. For example, the web browsing based on TCP. Indeed, uplink throughput distribution for MIMO 4×4 cells in band-3 is also slightly better than uplink throughput distribution for MIMO 2×2 cells (see orange and red lines) while no improvements are visible for cells in bands-7 (see light green and green lines).

6. Conclusion

The performance of MIMO 4×4 (with transmission mode 4) is measured in an RC set with different loading conditions. By means of absorbing material insertion and different stirrer rotating speeds, typical indoor and outdoor environments are reproduced. Realistic SINR values are also obtained with the aid of a wideband noise generator modulated with a duty cycle. The paper presents some results regarding the benefit of MIMO 4×4 introduction against MIMO 2×2 , in such replicated propagation environments. Such benefits are more remarkable for environments which are rich in multipath. However, when concentrating on MIMO 4×4 only, we realize how multipath may affect throughput performance, even if 4 transmitters and

4 receivers (thus complex diversity schemes) are used. The expected benefits from MIMO 4×4 activation could be a useful information for the operators that may want to provide additional radio capacity in some specific locations, despite the efforts needed for its implementation.

Acknowledgment

Authors would like to thank Raghunandan Udipi Diggavi of Qualcomm, Farnborough, UK for providing test devices and support in Extensible Diagnostic Monitor (QXDM).

References

- [1] D. A. Hill, Plane wave integral representation for fields in reverberation chambers, *IEEE Trans. Electromagn. Compat.* 40 (3) (1998) 209–217.
- [2] P. Corona, G. Ferrara, M. Migliaccio, Reverberating chambers as sources of stochastic electromagnetic fields, *IEEE Trans. Electromagn. Compat.* 38 (3) (1996) 348–356.
- [3] International Standards - IEC 61000-4-21, Geneva, Switzerland, Electromagnetic compatibility (EMC) - Part 4-21: Testing and measurement techniques - Reverberation chamber test methods, 2nd Edition (Apr. 2011).
- [4] C. Lötbäck Patané, A. Skårbratt, R. Rehammar, C. Orlenius, Basic and advanced MIMO OTA testing of wireless devices using reverberation chamber, in: *Proc. 8th Eur. Conf. Antennas Propag.*, The Hague, Netherlands, 2014, pp. 3488–3492. doi:10.1109/EuCAP.2014.6902581.
- [5] X. Chen, Measurement uncertainty of antenna efficiency in a reverberation chamber, *IEEE Trans. Electromagn. Compat.* 55 (6) (2013) 1331–1334. doi:10.1109/TEMC.2013.2265042.
- [6] 3GPP, Universal mobile telecommunications system (UMTS); LTE; universal terrestrial radio access (UTRA) and evolved UTRA (E-UTRA); user equipment (UE) over the air (OTA) performance; conformance testing, 3GPP Technical Specification TS37.544, V14.1.0, ETSI, Sophia Antipolis Cedex, France (Apr. 2017).
- [7] 3GPP, Verification of radiated multi-antenna reception performance of user equipment (UE) (release 12), 3GPP Technical Specification TR37.977, V12.1.0, ETSI, Sophia Antipolis Cedex, France (Mar. 2014).
- [8] P.-S. Kildal, C. Orlenius, J. Carlsson, OTA testing in multipath of antennas and wireless devices with MIMO and OFDM, *Proceedings of the IEEE* (7) (2012) 2145–2157. doi:10.1109/JPROC.2012.2188129.
- [9] N. Janssen, K. A. Remley, C. L. Holloway, W. F. Young, Correlation coefficient and loading effects for MIMO antennas in a reverberation chamber, in: *Int. Symp. Electromagn. Compat. (EMC EUROPE)*, Brugge, Belgium, 2013, pp. 514–519.
- [10] P.-S. Kildal, K. Rosengren, Correlation and capacity of MIMO systems and mutual coupling, radiation efficiency and diversity gain of their antennas: Simulations and measurements in reverberation chamber, *IEEE Commun. Mag.* 42 (12) (2004) 102–112.
- [11] C. M. J. Wang, K. A. Remley, A. T. Kirk, R. J. Pirkel, C. L. Holloway, D. F. Williams, P. D. Hale, Parameter estimation and uncertainty evaluation in a low Rician K-factor reverberation-chamber environment, *IEEE Trans. Electromagn. Compat.* 56 (5) (2014) 1002–1012. doi:10.1109/TEMC.2014.2313461.
- [12] C. S. Lötbäck Patané, A. Skårbratt, C. Orlenius, Extending the reverberation chamber using a channel emulator for characterisation of over-the-air performance of multiple-input–multiple-output wireless devices, *IET Science, Measurement Technology* 9 (5) (2015) 555–562. doi:10.1049/iet-smt.2014.0290.
- [13] A. Hussain, P.-S. Kildal, Study of OTA throughput of 4G LTE wireless terminals for different system bandwidths and coherence bandwidths in rich isotropic multipath, in: *Proc. 7th Eur. Conf. Antennas Propag.*, Gothenburg, Sweden, 2013, pp. 312–314.
- [14] D. Micheli, M. Barazzetta, F. Moglie, V. Mariani Primiani, Power boosting and compensation during OTA testing of a real 4G LTE base station in reverberation chamber, *IEEE Trans. Electromagn. Compat.* 57 (4) (2015) 623–634. doi:10.1109/TEMC.2015.2434277.
- [15] M. Barazzetta, D. Micheli, L. Bastianelli, R. Diamanti, M. Totta, P. Obino, R. Lattanzi, F. Moglie, V. Mariani Primiani, A comparison between different reception diversity schemes of a 4G-LTE base station in reverberation chamber: a deployment in a live cellular network, *IEEE Trans. Electromagn. Compat.* 59 (6) (2017) 2029–2037. doi:10.1109/TEMC.2017.2657122.
- [16] D. Micheli, M. Barazzetta, C. Carlini, R. Diamanti, V. Mariani Primiani, F. Moglie, Testing of the carrier aggregation mode for a live LTE base station in reverberation chamber, *IEEE Trans. Veh. Technol.* 66 (4) (2017) 3024–3033. doi:10.1109/TVT.2016.2587662.
- [17] International Telecommunication Union - ITU Report M.2135-1, Guidelines for evaluation of radio interface technologies for IMT-Advanced (Dec. 2009).
- [18] International Telecommunication Union - ITU Recommendation P.1238-7, Propagation data and prediction methods for the planning of indoor radiocommunication systems and radio local area networks in the frequency range 900 MHz to 100 GHz (Feb. 2012).
- [19] C. L. Holloway, H. A. Shah, R. J. Pirkel, K. A. Remley, D. A. Hill, J. Ladbury, Early time behavior in reverberation chambers and its effect on the relationships between coherence bandwidth, chamber decay time, RMS delay spread, and the chamber buildup time, *IEEE Trans. Electromagn. Compat.* 54 (4) (2012) 714–725. doi:10.1109/TEMC.2012.2188896.
- [20] X. Chen, P.-S. Kildal, C. Orlenius, J. Carlsson, Channel sounding of loaded reverberation chamber for over-the-air testing

MIMO 4x4 vs. MIMO 2x2 Performance Assessment of a Real Life LTE Base Station in a Reverberation Chamber

- of wireless devices: Coherence bandwidth versus average mode bandwidth and delay spread, *IEEE Antennas Wireless Propag. Lett.* 8 (2009) 678–681. doi:10.1109/LAWP.2009.2025149.
- [21] C. L. Holloway, D. A. Hill, J. M. Ladbury, P. F. Wilson, G. Koepke, J. Coder, On the use of reverberation chambers to simulate a Rician radio environment for the testing of wireless devices, *IEEE Trans. Antennas Propag.* 54 (11) (2006) 3167–3177.
- [22] K. A. Remley, R. J. Pirkl, C.-M. Wang, D. Senić, A. C. Homer, M. V. North, M. G. Becker, R. D. Horansky, C. L. Holloway, Estimating and correcting the device-under-test transfer function in loaded reverberation chambers for over-the-air tests, *IEEE Trans. Electromagn. Compat.* Accepted for publication, DOI: 10.1109/TEM.2017.2708985. doi:10.1109/TEM.2017.2708985.
- [23] E. Genender, C. L. Holloway, K. A. Remley, J. Ladbury, G. Koepke, H. Garbe, Use of reverberation chamber to simulate the power delay profile of a wireless environment, in: *Proc. IEEE Int. Symp. Electromagn. Compat.*, Hamburg, Germany, 2008, pp. 1–6. doi:10.1109/EMCEUROPE.2008.4786832.
- [24] O. Delangre, P. De Doncker, M. Lienard, P. Degauque, Delay spread and coherence bandwidth in reverberation chamber, *Electronics Letters* 44 (5) (2008) 328–329. doi:10.1049/el:20083676.
- [25] L. Bastianelli, L. Giacometti, V. Mariani Primiani, F. Moglie, Effect of absorber number and positioning on the power delay profile of a reverberation chamber, in: *2015 IEEE International Symposium on Electromagnetic Compatibility (EMC)*, Dresden, Germany, 2015, pp. 422–427. doi:10.1109/ISEMC.2015.7256199.
- [26] Y. Liu, X. Fang, M. Xiao, S. Mumtaz, Decentralized beam pair selection in multi-beam millimeter-wave networks, *IEEE Transactions on Communications* 66 (6) (2018) 2722–2737.
- [27] M. Xiao, S. Mumtaz, Y. Huang, L. Dai, Y. Li, M. Matthaiou, G. K. Karagiannidis, E. Björnson, K. Yang, C. I. A. Ghosh, Millimeter wave communications for future mobile networks, *IEEE Journal on Selected Areas in Communications* 35 (9) (2017) 1909–1935.